BEaTriX, the Beam Expander Testing X-ray facility for testing ATHENA's SPO modules: the collimating mirror

G. Vecchi, B. Salmaso, S. Basso, G. Sironi, M. Ghigo, et al.

G. Vecchi, B. Salmaso, S. Basso, G. Sironi, M. Ghigo, D. Spiga, E. Giro, G. Pareschi, G. Tagliaferri, "BEaTriX, the Beam Expander Testing X-ray facility for testing ATHENA's SPO modules: the collimating mirror," Proc. SPIE 11119, Optics for EUV, X-Ray, and Gamma-Ray Astronomy IX, 111191J (9 September 2019); doi: 10.1117/12.2530562

SPIE.

Event: SPIE Optical Engineering + Applications, 2019, San Diego, California, United States

BEaTriX, the Beam Expander Testing X-ray facility for testing ATHENA's SPO modules: the collimating mirror

G. Vecchi[1], B. Salmaso, S. Basso, G. Sironi, M. Ghigo, D. Spiga, E. Giro, G. Pareschi, G. Tagliaferri
INAF-Brera Astronomical Observatory, Via E. Bianchi 46, 23807 Merate, Lecco (Italy)

ABSTRACT

The BEaTriX (Beam Expander Testing X-ray) facility is now under construction at INAF-Brera Astronomical Observatory with the support of ESA. We aim to use it as a pathfinder to demonstrate the feasibility of the acceptance tests of the ATHENA's Silicon pore optics Mirror Modules (MM), i.e., point spread function and effective area measurements at two energies for all MMs. A microfocus X-ray source placed in the focus of a paraboloid mirror will provide a collimated X-ray beam to the next stages featuring the facility, i.e., the monochromator and the beam expansion units, which will finally enable the full illumination of the mirror modules under test. The collimating mirror has to satisfy severe surface specifications to allow the divergence of the X-ray beam reaching the requirements. Simulations, based on physical optics, have shown that the optical quality of the mirror surface has to reach 0.5 arcsec Half-Energy Width (HEW) at 4.51 keV. We procured a ground and lapped mirror substrate in HOQ 310 fused quartz material. The first step of the process is based on the bonnet polishing technology with our CNC IRP1200 Zeeko machine, and it is guided by the analysis of the metrological data obtained by the optical profilometer present at Media Lario S.r.l. laboratories. The spatial frequency errors not correctable by bonnet polishing can be then removed by smoothing and superpolishing processes, followed by ion beam figuring to correct the remaining errors in the low frequency range. In this paper, we report on the analysis performed to correlate the requirement on beam divergence to the manufacturing tolerances on the surface. We present the manufacturing process and the results so far achieved.

Keywords: ATHENA, BEaTriX, X-ray test facility, bonnet polishing, X-ray collimator, X-ray parabolic mirror

1. INTRODUCTION

ATHENA (Advanced Telescope for High-ENergy Astrophysics) is the second Large mission selected by ESA within the Cosmic Vision Program [1], with launch foreseen in 2031. The optics, based on Silicon Pore Optics (SPO) technology [2], consists of a large aperture X-ray mirror with a diameter of 2.4 m, effective area of 1.4 m^2 at 1 keV, and Half-Energy Width (HEW) of 5 arcsec at 1 keV [3]. The adopted modular architecture sets that 35 processed silicon plates are stacked into an X-ray Optical Unit (XOU). Four XOUs are aligned and integrated in the SPO Mirror Module (MM) using synchrotron radiation [4]. Acceptance tests of MMs are currently done at XPBF 2.0 and PANTER [5], although these facilities show limitations for testing the hundreds of MMs composing the mirror assembly module [6]. To overcome these limitations, INAF-Brera Astronomical Observatory started to design a pathfinder facility in 2012, BEaTriX (Beam Expander Testing X-ray), providing a broad (170 mm x 60 mm), uniform and parallel X-ray beam (divergence ≤1.5 arcsec HEW) at the energies of 1.49 and 4.51 keV [7-9]. The purpose of the BEaTriX facility, under realization with the support of ESA, is to carry out the acceptance tests (Point Spread Function (PSF) and effective area) of the ATHENA SPO MM's with the required accuracy, initially for the 4.51 keV energy, with later extension to 1.49 keV.

The optical design of BEaTriX is shown in Figure 1, and already presented in [6]. The source will be at the focus of the grazing incidence paraboloid mirror, with focal length of ~5 m and grazing incidence angle of 0.93 deg. The parallel X-ray beam emerging from the parabolic mirror is expanded in the vertical direction providing a section of 4 mm x 60 mm. The beam is then diffracted four times on Silicon crystals symmetrically cut with orientation (220). The resulting tight level of monochromation is necessary to minimize the effect of the energy dispersive properties of the beam

[1]gabriele.vecchi@inaf.it; phone +39 02 72320478; fax +39-02 72320601; www.brera.inaf.it

Optics for EUV, X-Ray, and Gamma-Ray Astronomy IX, edited by Stephen L. O'Dell, Giovanni Pareschi, Proc. of SPIE Vol. 11119, 111191J · © 2019 SPIE · CCC code: 0277-786X/19/$21 · doi: 10.1117/12.2530562

expander component [8]. Beam expansion in the horizontal direction is reached by an asymmetrically cut Silicon crystal (220) [10], producing a final beam of size 170 mm x 60 mm.

The collimating, parabolic mirror is one key element of the facility, and this paper focuses on its design and status of realization. Section 2 introduces to mirror design, reporting on the analysis that allowed translating the requirement on the X-ray beam divergence into the tolerances that surface manufacturing has to fulfill. Section 3 reports on the manufacturing process we planned for the mirror. We then describe the characteristics of the procured mirror blank, the metrology equipment and the results yet achieved using the bonnet polishing technique.

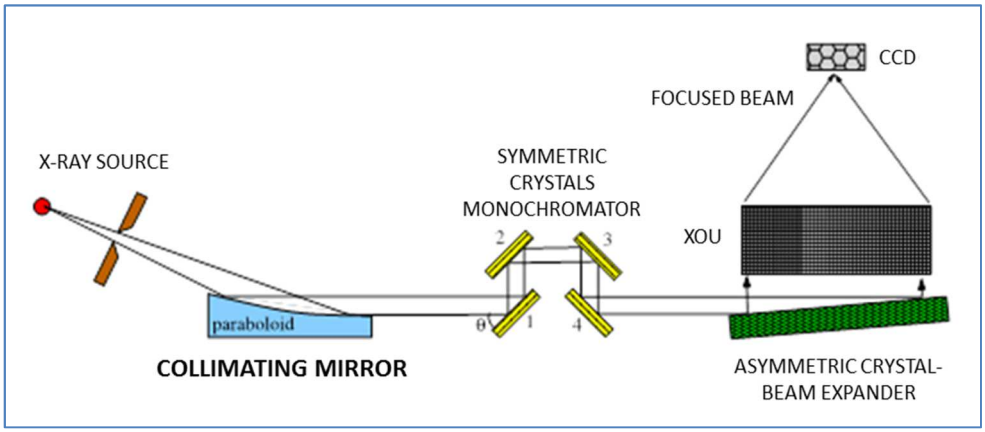

Figure 1. Optical design of the BEaTriX facility.

2. DESIGN OF THE COLLIMATING MIRROR

We evaluate the HEW error contribution of the mirror within the overall BEaTriX expected beam divergence. Modeling the Power Spectral Density (PSD) of the optical surface with a power law of the spatial frequency, we derive the tolerances that both surface figure and micro-roughness will have to satisfy to reach the required HEW specification.

2.1. Mirror requirements

In the HEW error budget for the ATHENA telescope, 4.3 arcsec were allocated for each MM [11]. Testing the MM with a collimated beam requires better collimation than 2 arcsec. Actually, the MM's PSF is almost monodimensional, and this is relevant for BEaTriX design, because a different behavior is expected in the vertical and horizontal divergence of the BEaTriX beam, due to the energy dispersive behavior of the asymmetric crystal [8]. Recent simulations [12] show that the beam divergence in BEaTriX would reach HEW-vertical = 0.8 arcsec and HEW-horizontal = 1.5 arcsec, by assuming that the parabolic mirror and its alignment are perfect, among other conditions [9].

Error budgeting has been performed [9] to account for the degradation of the beam collimation, which includes the non-perfect surface quality of the collimating mirror. Therefore, the expected divergence of BEaTriX beam in the vertical direction, the most critical for testing ATHENA MMs, is about 1.5 arcsec.

The dependence of the overall beam divergence upon the quality of the collimating mirror is fully described in [12] and shown in Fig.2. It can be seen that a surface quality of 0.5 arcsec HEW produces almost no degradation in the final beam divergence.

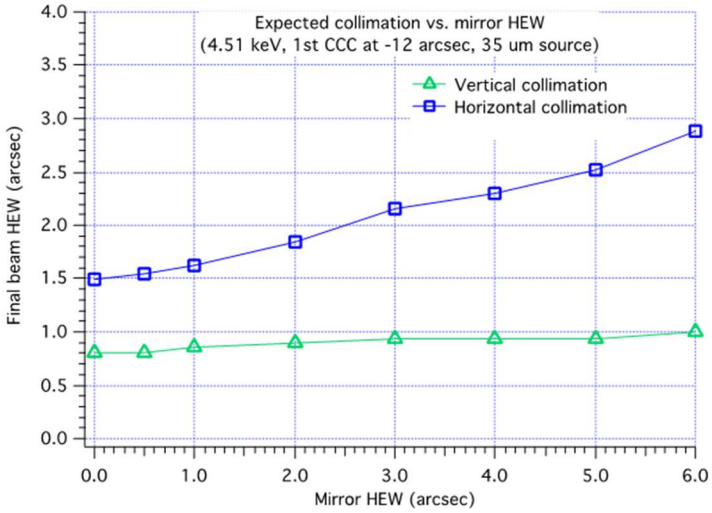

Figure 2. Dependence of the final beam divergence on the quality of the parabolic mirror, for a source of size 35 µm × 35 µm [12].

2.2. Manufacturing tolerances

To ensure a proper performance of BEaTriX , the surface quality of the collimating mirror is very important. In order to determine the manufacturing tolerances, the Wavefront propagatIon Simulation codE (WISE) code [13] was used to compute the maximum error in the figure and micro-roughness that is tolerable for a mirror of 0.5 arcsec HEW. The figure and micro-roughness profiles along the optical axis were generated from the mono-dimensional PSD described by the inverse power law-model:

$$PSD(f) = K_n / f^n \tag{1}$$

with $1<n<3$ and K_n constant [14]. Broken power laws were considered with knee at 1 mm, passing from figure to micro-roughness errors. In Fig.3, the three considered PSDs defined by different broken power laws are shown.

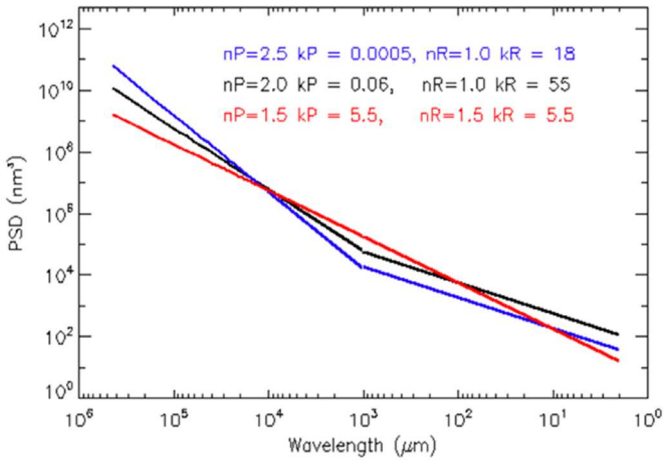

Figure 3. PSDs (in units of nm^3) for the figure and micro-roughness of the parabolic mirror: all three PSDs produce profiles with HEW < 0.5 arcsec. The values of nP, kP (nR, kR) selected for the figure Profile (micro-Roughness), respectively, are displayed.

The considered PSDs all return HEW < 0.5 arcsec at 4.5 keV, as shown in Table 1. The HEW values are computed with the WISE code, generating the longitudinal profile from the PSDs. The Root Mean Square (RMS) height and slope errors associated to the generated surface profile are also reported.

Table 1. HEW computed with the WISE code at 4.5 keV (both figure profile and micro-roughness errors are included).

Case	Profile		Micro-roughness		Total RMS [Å]	Slope RMS [µrad] (436 ÷ 1 mm)	HEW [arcsec]
	n	k	n	k			
A	2.5	0.0005	1.0	18	139	1.1	0.50
B	2.0	0.06	1.0	55	65.7	1.5	0.50
C	1.5	5.5	1.5	5.5	30.7	2.1	0.47

Table 2 reports the RMS errors computed from the PSDs in different spatial frequency ranges.

Table 2. Power law parameters and RMS values.

Case	Profile		Micro-roughness		RMS from PSD [Å] (436 ÷ 100 mm)	RMS from PSD [Å] (100 ÷ 10 mm)	RMS from PSD [Å] (10 ÷ 1 mm)	RMS from PSD [Å] (1 mm ÷ 10 µm)
	n	k	n	k				
A	2.5	0.0005	1.0	18	117.7	29.3	5.6	2.9
B	2.0	0.06	1.0	55	53.1	21.8	7.3	5.0
C	1.5	5.5	1.5	5.5	21.5	14.7	8.6	5.6

RMS values reported in Table 2 suggest that to polish a collimating mirror with such extremely high surface quality is a challenging objective.

3. MANUFACTURING OF THE COLLIMATING MIRROR

We plan a manufacturing process of the optical surface, in terms of both figure error and micro-roughness, based on the complementary techniques of bonnet polishing/figuring, pitch superpolishing and ion beam figuring. The superpolishing process is set to smooth both the mid- and the high-spatial frequency (micro-roughness) range of the surface error, which are very difficult to correct by the two other techniques. The deterministic processes like the bonnet polishing and ion beam figuring provide best correction capability in the low spatial frequency range, i.e., when the tool size is much smaller than the wavelength error. On the opposite, the figuring capability worsen progressively when the wavelength error approaches the tool/removal function size. We assumed, roughly, the onset of mid-frequency range at the wavelength error of 7 mm, where we found that the capability of error reduction by bonnet polishing becomes very poor. Setting this limit is useful for designing the smoothing tool, which will have to address surface ripples up to 7 mm long, with possible extension to ~10 mm. We foresee ion beam figuring being the last step of mirror manufacturing (excluding coating), addressing the remaining low frequency (figure) error expected after and/or caused by the smoothing and superpolishing processes. The following discussion will focus on the bonnet polishing results so far achieved.

3.1. Procurement of mirror blank

We procured two mirror blanks in fused quartz HOQ 310 from Carl Zeiss SMT GmbH. Fig.4 shows one of two parabolic mirror blanks at Zeiss. One blank was ground to the nominal shape with requested Peak-to-Valley (PV) figure accuracy < 15 µm, and micro-roughness with RMS < 2 µm. This blank has been regarded so far as a spare part, whilst, for future development of the facility, it is planned as the collimating mirror in the 1.49 keV beamline. The second mirror blank, object of the present work, was ground and lapped to the requested shape with PV accuracy < 5 µm and RMS < 0.5 µm for the micro-roughness. The lapping process is convenient to reduce the remaining error after grinding and to remove most of the subsurface damages due to grinding. The resulting surface is opaque and ready for polishing.

Figure 4. Mirror blank manufactured at Carl Zeiss SMT GmbH.

Fig.5 shows a drawing of the grazing incidence paraboloid mirror. Size and radii of curvature are also reported, varying from 153.5 mm at the entrance of the X-ray beam (4.75 m away from the X-ray source) to 160.4 mm at the opposite edge of the clear aperture. The size of the workpiece is 456 mm × 100 mm × 50 mm, it was ground to the area of 456 mm × 80 mm, while the 436 mm × 60 mm area refers to the optical surface of the mirror. The workpiece thickness is bigger (50 mm) at the side of the smallest radius than at the opposite side (49.75 mm). The two flat surfaces at the front side are not parallel to the backside of the substrate. Instead, the backside is parallel to the straight line that approximates the generatrix (central profile) of the paraboloid surface.

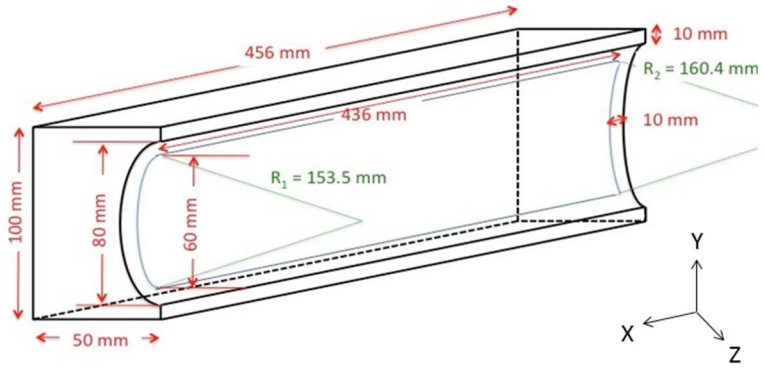

Figure 5. Drawing of the workpiece with indication of size, radii of curvature and axes system.

The residual error in the shape of the mirror blank after lapping was measured at Zeiss with a highly accurate coordinate measuring machine (UPMC 850 CARAT). The longitudinal error map is shown in Fig.6, displaying ~3.1 µm PV. The micro-roughness of the lapped surface was measured using a roughness measuring machine (Surfcom 130A), leading to values Rq<0.4 µm, meeting the requirements.

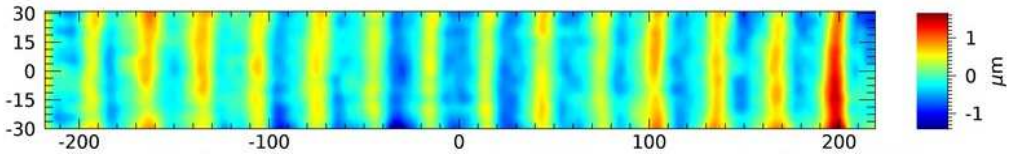

Figure 6. Longitudinal error map of the incoming mirror blank measured at Carl Zeiss SMT GmbH. The map covers the 436 mm x 60 mm optical area. The PV (RMS) error is ~3.1 µm (~0.4 µm).

We set the free-form optical profilometer/rotondimeter MPR-700 available at Media Lario S.r.l. [15] as the baseline equipment to measure the shape accuracy of the mirror surface, and to track its improvement during the polishing/figuring corrective process. We designed and manufactured an interfacing structure in Aluminum to the rotational table of the MPR-700, with the mirror supported on a 3-points kinematic mount, by means of three pads fixed on its side using a vacuum compliant glue (Masterbond EP-30). The interfacing structure includes a weight to counterbalance the mirror weight during rotations. We performed finite element analysis to account for the displacement of the whole system (including the mirror) upon the influence of gravity, when coupled to the profilometer system. We aligned the parabolic mirror with respect to the rotational axis of the optical profilometer by using a coordinate measuring machine. Fig.7 shows the mirror in the MPR-700 profilometer. We measured several longitudinal profiles of the surface, by rotating the MPR-700 table, to cover the area 436 mm × 60 mm of the optical surface. Longitudinal profiles were acquired with 0.1 mm sampling, and interpolated to 1 mm resolution, more than enough for correcting the figure error with wavelength several millimeters long. Data reduction included an

optimization routine to let the measured residuals unaffected by the repositioning error of the mirror substrate on top of the MPR-700 system. After an assessment of the azimuthal (sagittal) error, we decided to address the longitudinal (axial) error only. This is a common assumption for grazing incidence X-ray optics, where the longitudinal profile error dominates the PSF broadening.

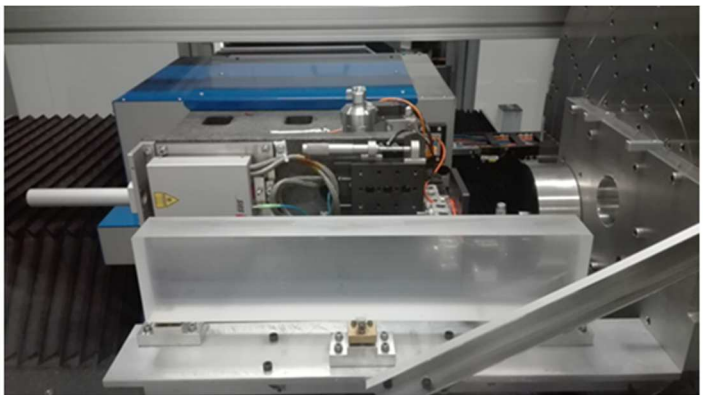

Figure 7. Workpiece mounted on the MPR-700 optical profilometer at Media Lario S.r.l.

3.2. Bonnet polishing

We started the polishing of the parabolic mirror employing an IRP1200 machine by Zeeko Ltd [16]. The machine is available at INAF-Brera Astronomical Observatory and implements the bonnet polishing technique. Fig.8A shows the mirror mounted on the machine in preparation for polishing. The IRP1200 machine makes use of a sub-aperture rubber tool, the so-called bonnet, to polish the surface and correct its error shape while it is scanned following a defined path. The bonnet is inflated by air pressure and is typically dressed with a polyurethane foil. An abrasive slurry, often based on cerium oxide for glass, is delivered to the workpiece-tool contact area. Fig.8B shows a picture taken during polishing. The mirror is not visible as the recirculating slurry flushes it.

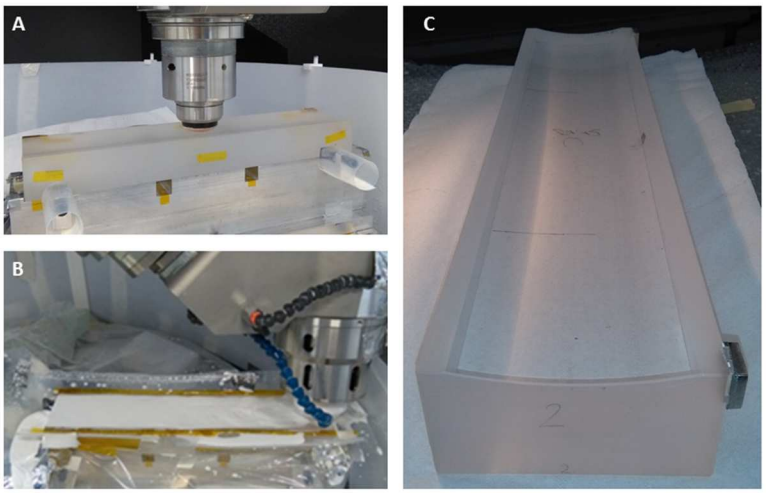

Figure 8. A. The parabolic mirror mounted on the IRP-1200 Zeeko machine. B. Running the bonnet polishing: the optical surface is underneath the recirculating abrasive slurry. C. The glossy optical surface after bonnet polishing. One of the three pads glued on the side of the workpiece is visible.

Removal of glass follows the Preston model [17], and is proportional to the time the tool is spending at each position on the surface. A dwell time matrix is calculated in order to correct the measured error map of the surface. The machine executes a dwell time matrix by continuously changing the tool speed along the path. The smallest size of bonnet available can address figure error with spatial wavelength down to the 10 mm range. However, the polishing technique using a compliant rubber-based tool is less efficient in this range. Depending on the specific surface requirements, it

may become convenient to operate other kind of tools, better suited to flatten surface undulations of this and shorter wavelength range [18]. We present here the results achieved so far with the bonnet polishing process.

At first, we ran 5 cycles of uniform polishing over the lapped surface of the mirror blank. This part of the process aimed at removing most of the layer depth where the presence of residual subsurface damages is expected. We estimated an overall removal of about 15 µm of glass. We were applying a bonnet whose size and offset were providing a contact spot of ~10 mm diameter, and we polished this way for an overall time of about 25 hours. The optical surface started to look glossy already after the first 5 hours of polishing: a picture of the workpiece after 25 hours of polishing is shown in Fig.8C. The longitudinal error map obtained from the optical profilometry at the end of uniform polishing series is displayed in Fig.9 (top panel). The central longitudinal profile from this map is shown (in red color) in Fig.9 (bottom panel), and compared to the central profile (in blue color) extracted from the error map in Fig.6, related to the lapped surface. The uniform polishing did not affect the dominant undulation, as expected, whereas it introduced a sag term, leading the RMS error to increase from ~0.4 µm to ~0.55 µm.

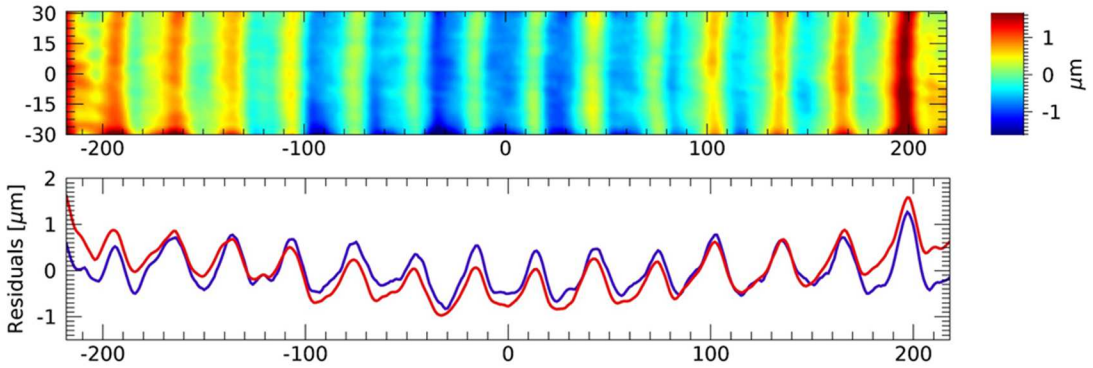

Figure 9. (top) Longitudinal error map after ~25 hours of uniform polishing. The RMS value is ~0.55 µm. (bottom) Comparison of central profiles extracted from the error map in this figure (red) and from the initial error map in Fig.6 (blue).

Afterwards, we started to figure the glass surface by modulating the speed of the scanning tool (same bonnet as in previous uniform polishing) according to the error map in Fig.9 (top). After two cycles, each one less than 3 hours long, we measured the error map shown in Fig.10, with the corresponding RMS value of ~0.1 µm.

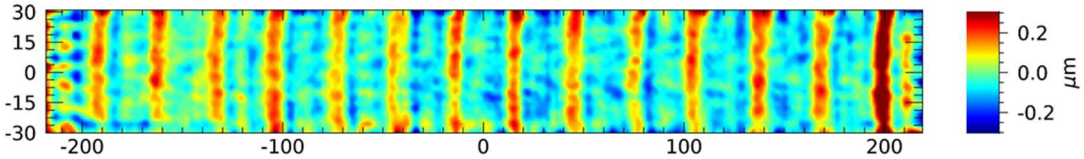

Figure 10. Longitudinal error map after two cycles (less than 6 hours overall time) of figuring, with RMS error decreased to ~0.1 µm.

We changed the size of the bonnet to keep on the convergence of the figuring process, moving to a smaller contact spot of ~5 mm diameter. By three cycles and overall polishing time of about 11 hours, we reached a longitudinal error of ~0.05 µm (RMS). In the residual error map shown in Fig.11 (top panel) the main ripple caused by grinding has been mostly removed. The central longitudinal profile from this map is shown (in red color) in Fig.11 (bottom panel), and compared to the central profile (in blue color) extracted from the error map in Fig.10, after the first corrective series which used the larger bonnet.

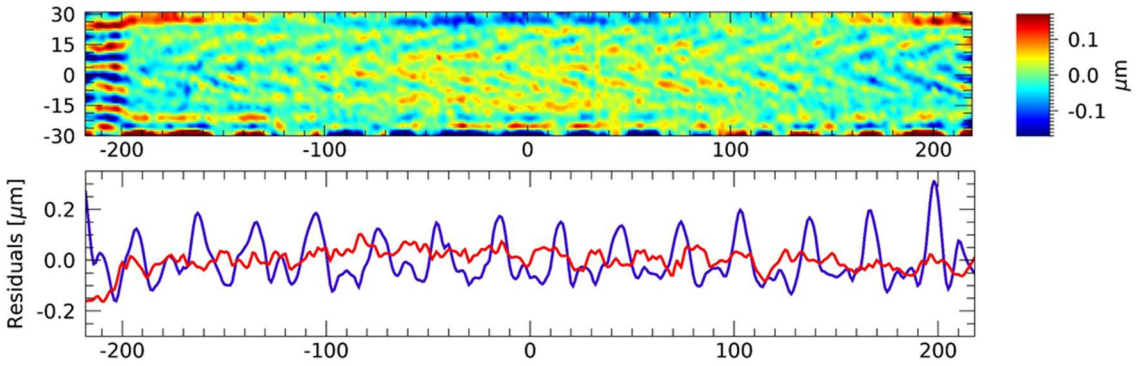

Figure 11. (top) Longitudinal error map after three cycles (~11 hours overall time) of corrective polishing with a smaller bonnet, with RMS error decreased to ~0.05 µm. (bottom) Comparison of central profiles extracted from the error map in this figure (red) and from the error map in Fig.10 (blue).

We show in Fig.12 the PSDs calculated from the longitudinal error measured after uniform polishing (map in Fig.9 (top panel)), after the first corrective series (map in Fig.10) and after the second corrective series with smaller bonnet (map in Fig.11 (top panel)). In the same chart, we also display the PSD requirements for achieving HEW values of 0.5 arcsec (goal) and 1 arcsec. On the long wavelength side, we reached the PSD requirement corresponding to 1 arcsec HEW so far. The peak at wavelength near 30 mm, dominant the PSD of the incoming map of mirror blank, was largely decreased after corrective polishing. In order to reach the PSD requirement at this wavelength and, generally, in the range above 10 mm we plan to address the remaining error by using the ion beam figuring technique. For the correction of residual error in the wavelength range < 10 mm we are developing a smoothing process with dedicated pitch tool. We plan to use the same tool also for the superpolishing.

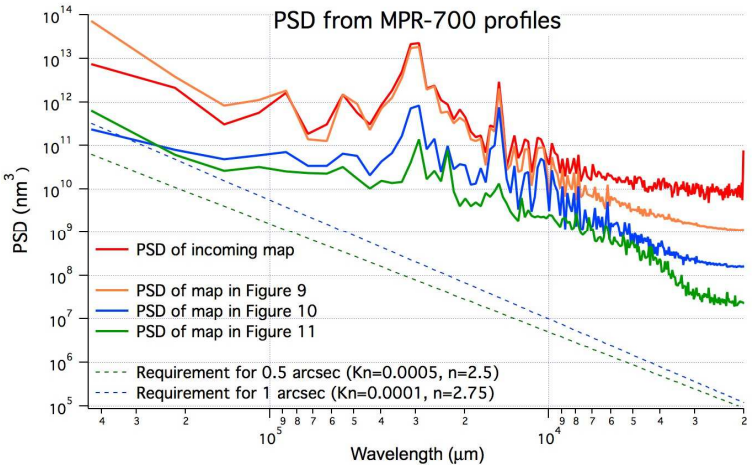

Figure 12. PSDs calculated from the longitudinal error maps at incoming of mirror blank, after uniform polishing (Fig.9), first series of figuring (Fig.10) and second series of figuring (Fig.11). PSD requirements for 0.5 and 1 arcsec HEW are also shown for sake of comparison.

4. CONCLUSION

In this paper, we presented the geometrical characteristics and the optical tolerances of the paraboloid grazing incidence mirror of the BEaTriX facility under construction at INAF-Brera Astronomical Observatory. The mirror was designed to ensure both collimation and expansion in the vertical direction of the BEaTriX beam, suited for X-ray acceptance tests of ATHENA's SPO MMs. A severe error budgeting for beam divergence has resulted in tight tolerances for the optical surface, therefore, in a challenging fabrication job. We planned to tackle the task by splitting the manufacturing process over three main complementary steps, each one defined by a different polishing/figuring technique: bonnet

polishing, pitch smoothing/superpolishing and ion beam figuring. In this work, we reported on the bonnet polishing technique and the related results so far achieved. We improved the figure accuracy lowering the residual error from the value of ~0.55 µm (RMS) measured after uniform polishing to ~0.05 µm (RMS) after 5 cycles of corrective polishing (figuring). This was performed over the 436 mm × 60 mm area of the paraboloid optics. The work is ongoing to fulfill the tight tolerances required by the design of the BEaTriX facility.

ACKNOWLEDGMENTS

The development of the BEaTriX facility is funded by the ESA contract No. 4000123152/18/NL/BW, "Advanced and Compact X-ray Test facility for the ATHENA SPO module. We thank M. Rossi and L. Arcangeli (Media Lario S.r.l.) for technical support and P. Conconi for useful discussions.

REFERENCES

[1] Nandra, K., Barret, D., Barcons, X., et al., "The Hot and Energetic Universe: A White Paper presenting the science theme motivating the Athena mission," http://arxiv.org/abs/1306.2307 (2013).
[2] Collon, M., Vacanti, G., Barriere, N., Landgraf, B., Guenther, R., et al., "Silicon pore optics mirror module production and testing," Proc. SPIE 10699, 106990Y (2018).
[3] Bavdaz, M., Wille, E., Ayre, M., Ferreira, I., Shortt, B., et al., "Development of the ATHENA mirror," Proc. SPIE 10699, 106990X (2018).
[4] Krumrey, M., Muller, P. et al., "New X-ray parallel beam facility XPBF 2.0 for the characterization of the silicon pore optics," Proc. SPIE 9905, 99055N (2016).
[5] Vacanti, G., Collon, M.J., Barrière, N.M., Landgraf, B., Günther, R., et al., "X-ray testing of Silicon Pore Optics," Proc. SPIE this conference.
[6] Salmaso, B., Spiga, D., Basso. S., Ghigo, M., Giro, E., Pareschi, G., Tagliaferri, G., Vecchi, G., et al., "Progress in the realization of the beam expander testing x-ray facility (BEaTriX) for testing ATHENA's SPO modules," Proc. SPIE 10699, 1069931 (2018).
[7] Spiga, D., Pareschi, G., Pelliciari, C., et al., "Functional tests of modular elements of segmented optics for x-ray telescopes via an expanded beam facility," Proc. SPIE 8443, 84435F (2012).
[8] Spiga, D., Pelliciari, C., Salmaso, B., et al. "Design and advancement status of the Beam Expander Testing Xray facility (BEaTriX)," Proc. SPIE 9963, 996304 (2016).
[9] Salmaso, B., Basso, S., Giro, E., Spiga, D., Sironi, G., Vecchi, G., Ghigo, M., Pareschi, G., Tagliaferri G., et al., "Progress in the realization of the beam expander testing x-ray facility (BEaTriX) for testing ATHENA's SPO modules," Proc. SPIE this conference.
[10] Sanchez del Rio, M., Cerrina, F., "Asymmetrically cut crystals for synchrotron radiation monochromators," Review of Scientific Instruments 63, 936 (1992).
[11] ATHENA CDF study report. Assessment of an X-ray telescope for the ESA Cosmic Vision Program, (2014).
[12] Spiga, D., Salmaso, B., Basso, S., Bavdaz, M., Burwitz, V., et al., "Optical simulations for the laboratory-based expanded and collimated x-ray beam facility BEaTriX," Proc. SPIE this conference.
[13] Raimondi, L., Spiga, D., "Mirrors for X-ray telescopes: Fresnel diffraction-based computation of point spread functions from metrology," A&A 573, A22 (2015).
[14] Church, E. L., "Role of surface topography in X-ray scattering," Proc. SPIE 184, 196-202 (1979).
[15] Sironi, G., Citterio, O., Pareschi, G., Negri, B., Ritucci, A., Subranni, R., Orlandi, et al., "MPR: innovative 3D free-form optics profilometer," Proc. SPIE 8147, 814718 (2011).
[16] Vecchi, G., Basso, S., Civitani, M., Ghigo, M., Pareschi, G., Riva, M. and Zerbi, F. M., "A bonnet and fluid jet polishing facility for optics fabrication related to the E-ELT," Mem. S.A.It. 86, 408 (2015).
[17] Preston, F. W., "The theory and design of plate glass polishing," Journal of the Society of Glass Technology 11, 214-256 (1927).
[18] Kim, D. W. and Burge J. H., "Rigid conformal polishing tool using non-linear visco-elastic effect," Opt. Express 18, 2242-2257 (2010).